Theoretical Investigations of Oxygen-17 NMR Chemical Shifts to Discriminate among Helical Forms

Itzam De Gortari,*,† Marcelo Galván,‡ Joel Ireta,§ Matthew Segall,† Chris J. Pickard,† and Mike Payne†

TCM Group, Cavendish Laboratory, University of Cambridge, Madingley Road, Cambridge CB3 0HE, United Kingdom, Departamento de Química, División de Ciencias Básicas e Ingeniería, Universidad Autónoma Metropolitana, A.P. 55-534, México 09340, and Fritz-Haber-Institut der Max-Planck-Gesellschaft, Faradayweb 4-6, D-14195 Berlin-Dahlem, Germany

Received: July 3, 2007; In Final Form: September 17, 2007

^{17}O, ^{15}N, ^{13}C, and ^{1}H NMR chemical shieldings are calculated using density functional theory to differentiate among the three primarily helical forms, 3_{10}, α, and π in polyalanine peptides under periodic boundary conditions. This study suggests ^{17}O as the best observable, as it has been demonstrated to be sensitive to hydrogen bonding and highly affected by small changes in the polypeptide in helix conformations. This theoretical study seeks to characterize the subtle conformational differences of helical structures by NMR chemical shift observables which may lead to important questions in experimental structure determination on the basis of using chemical shifts to identify protein secondary structures.

1. Introduction

When attempting to determine the structure of a protein by nuclear magnetic resonance (NMR), it is fundamental to know the effects of structural but minor changes in experimental observables. Helical secondary structures, for example, are differentiated from β strands in globular proteins by changes in ^{13}C chemical shifts. However, minor structural changes between different helical structures characterized by NMR observables has proven to be a difficult task since π and 3_{10} helices have seldom been reported. Crystal structures of proteins, on the contrary, have characterized the abundance of these different helical conformations, the α helix being the most prominent helical motif (about 80%) followed by the 3_{10} helix (about 20%).[1] The π helix is only rarely found.[2] Molecular dynamics (MD) studies of peptides initially containing α-helical structures have, however, yielded significant populations of π helices.[3] For noncrystallised proteins, there is no a comparable study on the occurrence of helical types because of the experimental difficulty in distinguishing between different helical motifs.

NMR chemical shifts are a fingerprint of protein structure, but to link these observables to structural information, a number of technological limitations must be overcome. For the case of the three different helical structures, present experimental NMR techniques have reached their limits and are unable to differentiate between them; nuclear Overhauser effect (NOE) experiments cannot confidently exclude the presence of significant π helix in a peptide because of its limitation in obtaining accurate interatomic distances.[4] Distance measurements with this technique give the same values for both the α and π helices. Also, these experiments cannot take into account dynamic fluctuations and possible bifurcated hydrogen-bonding patterns. Other protein structure investigations by NMR have derived information from the scalar coupling and dipolar interactions to point out differences between helices.[3] These were by looking at the coupling across hydrogen bonds; however, intra-residue coupling has been estimated to be on the same order of magnitude as the coupling across the hydrogen bonds.[5]

The common consensus is that the most effective way to use NMR to distinguish among helices is by probing their hydrogen-bonding patterns, as these are important for stabilizing the helical conformations and the transition states that occur during the structural interconversion between helices.[6] Here, this previous assumption is evaluated by a theoretical study based on recent developments to obtain reliable NMR parameters within a total energy pseudopotential method[7] and periodic boundary condition framework. In this theoretical study, the limitation of looking at observables like $^{13}C^{\alpha}$,$^{13}C^{\beta}$,$^{13}C^{O}$, and ^{15}N chemical shifts is clear, and it is suggested that ^{17}O chemical shift anisotropy (CSA) is the most sensitive tool to identify the most subtle changes in helical conformations. It will be shown that a correlation between anisotropic chemical shifts and helical conformation parameters in periodical structures of polylalanine is feasible. Thus, we take advantage of these developments to determine differences in the chemical shifts between the common helical structures, α, π, and 3_{10} helix, in proteins.

Contributions to the chemical shifts have been studied since 1993. Oldfield's group published the first work in that the secondary and intermolecular contributions to theoretical shieldings were obtained.[8] In this context, solvent effects play an important role in accurately calculating NMR chemical shifts. In order to make a comparison while controlling as many variables as possible, this study is restricted to a model in which the boundary and solvent effects are omitted. It is well-known from the study of capped helical polypeptides that the boundary effects can be significant.[9] In this study, boundary effects are

* Corresponding author. E-mail: dego@nmr.mpibpc.mpg.de. Current address: Department for NMR Structural Biology, Max-Planck-Institute for Biophysical Chemistry, Am Fassberg 11, 37077 Goettingen, Germany

† University of Cambridge.

‡ Universidad Autónoma Metropolitana.

§ Fritz-Haber-Institut der Max-Plank-Gesellschaft.

10.1021/jp0751817 CCC: $37.00
Published on Web 11/17/2007

avoided by using a periodic polymeric model that, in addition, provides an upper limit for hydrogen bond cooperativity. The latter is crucial for stabilizing the bulk of a helical conformation.[10−12] Infinite-chain models, which enable us to focus on the properties of the center (bulk) of a helix, have been shown to properly describe helical conformations.[13,14] Thus, by omitting solvent interactions, one can be certain that NMR chemical shift differences between helical structures are purely due to conformational effects.

NMR chemical shifts were calculated for α, π, and 3_{10} helical and fully extended (also known as single strand β-sheet) structures of an infinitely long polyalanine chain. These structures are minima in the potential energy surface (PES).[6] Similarly, chemical shifts were calculated for helical conformations along the PES, including the transition state structures and intermediate conformations. Accordingly, the models used in this work were optimized while only restricting the system in order to retain helical symmetry. The information extracted from NMR calculations relies on the quality of refinement of the structures, highly refined structures allow us to evaluate sensitivity of chemical shieldings to minor changes in the helical structures. Polyalanine was selected because there is much experimental information available for this system in solid and liquid phases[15−17] and because alanine is not a β-branched amino acid.[18] The latter point is important because the behavior of its NMR shielding tensor is representative of the great majority of amino acids that have double substitution in their β carbon atoms.

2. Computational Methods

DFT Procedures. All of the electronic structure calculations were performed within the framework of density functional theory in its Kohn−Sham relation.[19] The ab initio total energy pseudopotential approach with plane wave basis sets was used to determine ionic positions corresponding to the minima in the potential energy surface. As the system under study requires an accurate description of hydrogen bonds, the generalized gradient approximation for the exchange correlation potential of Perdew−Burke−Ernzerhof (PBE) was employed.[20] This exchange and correlation potential allows not only a good description of the hydrogen bonds but also provides an accurate evaluation of NMR parameters. The truncation of the plane wave expansion uses a cutoff energy of 70 Rydbergs (Ry), and the Brillouin zone was sampled at the Γ point, except for the β or full extended structure (FES) where two k points were found to be necessary to achieve energy convergence. Pseudopotentials of the Troullier−Martins[21] type were used, and the energy and geometrical minimizations were performed within the parallel version of the FHIMD code.[22]

NMR Calculations. The chemical shielding was calculated using PARATEC[23] for all atoms using norm-conserving Troullier−Martins pseudopotentials within the gauge including projector augmented wave method (GIPAW).[7] To be consistent with the method used to minimize the structures, the same pseudopotentials were used, and the same PBE general gradient approximation was used as in the geometry optimization. The energy cutoff for the plane wave basis set for these calculations was 90 Ry, which is required to properly calculate ^{17}O chemical shifts. The integrals over the Brillouin zone were performed using one k point of (1/4, 1/4, 1/4). The accuracy of these Brillouin zone integrations was verified by using a different set of k points in the Monkhorst−Pack framework.[24] In this work, referenced values of NMR chemical shifts δ are presented and follow to the chemical shielding (σ) Haeberlen scheme.[25]

TABLE 1: Reference Values σ_{ref} and Experimental δ_{iso} for Different Nuclei in α Helical Conformation

	σ_{ref}	δ_{iso}^{exp}
σ^1H	29.55	8.21[a(9)]
σ^{13}C	168.62	53.2[b(16)]
σ^{15}N	194.45	98.8[c(17)]
σ^{17}O	232.28	319[d(42)]

[a] $^1H^N$ chemical shift obtained in water-solubilized helical polylalanie. [b] $^{13}C^\alpha$ chemical shift obtained from polyalanine powder. [c] ^{15}N chemical shift obtained from solid-state (ss) NMR experiments. [d] ^{17}O chemical shift obtained from ssNMR experiments.

The isotropic shielding is

$$\sigma_{iso} = \frac{1}{3}(\sigma_{11} + \sigma_{22} + \sigma_{33}) \quad (1)$$

where σ_{11}, σ_{22}, and σ_{33} are the eigenvalues of σ and are ordered as

$$\sigma_{33} \geq \sigma_{22} \geq \sigma_{11} \quad (2)$$

All theoretical values presented here were obtained from the nuclear shielding tensor connected to the magnetic field by the relation $B_{in}(r) = -\hat{\sigma}(r)B_{ext}$; its isotropic trace is $\sigma(r) = Tr[\hat{\sigma}]/3$. These theoretical quantities can be compared with experiment after referencing to the appropriate scale.[26] For future comparison, one obtains the isotropic chemical shift by $\delta_{iso} = -(\sigma_{iso} - \sigma_{ref})$. For each nucleus, σ_{ref} is chosen such that the calculated and experimental chemical shifts in α helix in polyalanine coincide. This procedure does not introduce inconsistencies as differences among structures are being compared. Table 1 shows σ_{ref} for all nuclei with their respective experimental values.

Chemical shielding (σ) and chemical shift (δ) cannot be directly compared. On one hand, the chemical shielding is a molecular electronic property; on the other, the chemical shift is a experimental quantity measuring the absolute shielding value. In this context, values which are independent from experimental references are the span Ω and skew κ defined as

$$\Omega = (\sigma_{33} - \sigma_{11}) \quad (3)$$

and

$$\kappa = 3(\sigma_{22} - \sigma_{iso})/(\sigma_{33} - \sigma_{11}) \quad (4)$$

The span is always a positive quantity and corresponds to the width of the resonance, whereas the skew is positive when the resonance reaches a maximum. In this way, κ and Ω are independent of the experimental reference.

For the case of ^{17}O, electric field gradients (EFGs) acting on this nucleus were calculated using the PARATEC code with the method described elsewhere.[27] The quadrupolar coupling constant C_Q and the asymmetry parameter η_Q were extracted from the diagonalized EFG tensor whose eigenvalues are labeled V_{xx}, V_{yy}, and V_{zz} such that $|V_{xx}| > |V_{yy}| > |V_{zz}|$, and are given by

$$C_Q = eV_{zz}Q_O/h \quad (5)$$

where h is Planck's constant and

$$\eta_Q = (V_{xx} - V_{yy})/V_{zz} \quad (6)$$

The experimental value used for the electric quadrupole moment of the oxygen nucleus is $Q_O = 2.55$ fm^2.[28]

Validation. The approach used to obtain the NMR parameters has been extensively tested by direct comparison with experi-

TABLE 2: Comparison between Theoretical and Experimental Values of $^{13}C^{O}$ and ^{15}N (δ) Chemical Shifts in L-alanyl-L-alanine Crystalline Powder Samples as in Ref 31 and the Anisotropic Tensor Angles (CSA$\angle$), the Span (Ω), and the Skew (κ)

	C^{O}		N	
L-alanyl-L-alanine	exptl[43]	theory	exptl[43]	theory
δ	170	170.38	−260	−262.76
CSA$\angle$	39.5[a]	38.38	106[b]	99.3
Ω[c]	149	152.4	150.2	193.99
κ[d]	0.018	−0.038	0.83	0.79

[a] $\angle(\sigma_{11}, \overrightarrow{C^{O}N})$. [b] $\angle(\sigma_{33}, \overrightarrow{NC^{O}})$. [c] $\Omega = \sigma_{33} - \sigma_{11}$. [d] $\kappa = 3(\sigma_{iso} - \sigma_{22})/(\sigma_{33} - \sigma_{11})$

ment and other results in the literature,[27,29,30] and it has been shown that good agreement with experiment relies on the quality of the input structure. There is still no clear consensus whether ab initio methods for NMR chemical shift calculations return better results for solution or solid state. In the case of the crystal, the packing interaction and its periodicity involves a well-defined static environment for each molecule. Additionally, anisotropic parameters can be extracted from solid-state (ss-NMR) experiments, and these offer more information about the structure of the crystal. In solution, there is greater structural uncertainty in the molecule, yet the spectrum describes the average of a range of possible conformations, and therefore structural errors cancel.

A comparison of our calculations with experimental data was carried out for polycrystalline L-alanyl-L-alanine (AA).[31] Hydrogen positions in X-ray crystals structure are poorly determined; for this reason, all protons were relaxed in the crystal while the remaining atoms were kept fixed. Table 2 shows the computed $^{13}C^{O}$ (carbonyl carbon) and ^{15}N NMR chemical shifts (δ) referenced to tetramethylsilane (TMS, $\sigma^{ref}(^{13}C) = 169.5$ ppm) and nitromethane (CH_3NO_2, $\sigma^{ref}(^{15}N) = -154.5$ ppm)[32] respectively for AA in the crystalline phase. The agreement with experiment for $^{13}C^{O}$ is remarkably good, even for the case of δ^{15} N where there is an error of 2.72 ppm. Table 2 also presents a comparison of the angles between main components of the chemical shift anisotropy (CSA) and molecular bonds, and similar to δ, a good agreement for $^{13}C^{O}$ and a small difference for ^{15} N are observed. These parameters can give crucial information about the packing in the crystal and represents a more complete set of observables than just the isotropic chemical shifts. Finally, in the same table, we present a comparison of the two experimental parameters, the span Ω and the skew κ, whose error with respect to experiment is larger for both nuclei $^{13}C^{O}$ and ^{15}N. The extremely large discrepancy between measured and calculated values of ω for ^{15}N can be related to the arbitrary selection of σ_{11} in the experiment. Since in the ^{15}N static spectra, the peak associated with the main components of the 2nd rank tensor is not easily defined, an improper representation of the span ω could be done. Further comparison between theory and experiment will need to be done to prove this hypothesis.

3. Helix Structures

To extract information out from predictions of NMR chemical shielding, a high resolution of the geometry of the system to be studied is needed. Therefore, special care was taken while studying the helical conformational map. The infinite α ,π, and 3_{10} helices were modeled in the orthorhombic supercells (a x a x c) with the helical axis parallel to the "c'' lattice side. The lattice parameter "a'' was fixed to minimize the interactions between the periodic images of the helix. The three structures

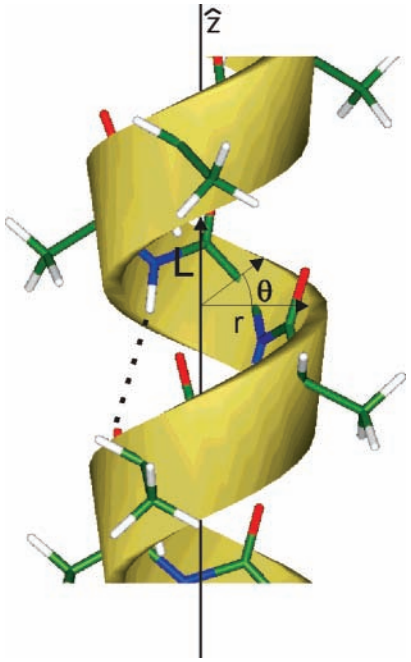

Figure 1. Scheme of the helix structure formation showing: "*L*'', the helix length per peptide unit measured along the helix axis; θ, the helix twist cycle; and "*r*'' the helix radius.

used were obtained by minimizing the energy of the ionic system with the only constraints being the helical symmetry. Thus, the geometry of the helices that minimize the energy were obtained by exploring the potential energy surface along two degrees of freedom: (a) *L*, the helix length per peptide unit, measured along the helix axis, and (b) θ, the helix twist. Both are illustrated in Figure 1. For each point in the $\{L, \theta\}$ space, the energy was minimized with respect to the positions of the atoms in the peptide unit while maintaining helical symmetry. In this scheme, the standard torsion angles of the Ramachandran plot, ϕ and ψ, result from the minimization procedure allowing the angle ω to vary.

The twist θ depends on the number of peptide units per supercell *N* and on the number of helix turns per supercell *m* according to the relation $\theta = 360° \, m/N$. Hence, as *m* must be an integer to satisfy the periodic boundary conditions, the sampling procedure implies the use of different values of *N*. The corresponding *L*, *N*, and θ values for the minimum energy structures are shown in Table 3, as well as the data for the minima in an infinitely and fully extended structure (FES) representing an isolated β strand conformation. This FES structure was obtained by a complete minimization of the energy with respect to all of the atom positions in the unit cell. Complete details of the potential energy surface of the helical structures have been published elsewhere.[6] There are no directly comparable theoretical results, as all previously published results were calculated for small model peptides.

4. Results and Discussion

Isotropic Chemical Shift. The isotropic chemical shifts were calculated for the main atoms of the peptidic unit in each helical structure and the fully extended structure; these are plotted in Figure 2. All of the values in this graph are referenced, as explained before, with the σ_{ref} shown in Table 1. For π, α, and 3_{10} structures, all four nuclei offer a poor systematic way to differentiate between them. First, ^{15}N and ^{1}H chemical shifts of the three minima follow an almost horizontal line within the plot. Second, δ ^{13}C of carbon-α , -β, and -C^{O} has the largest

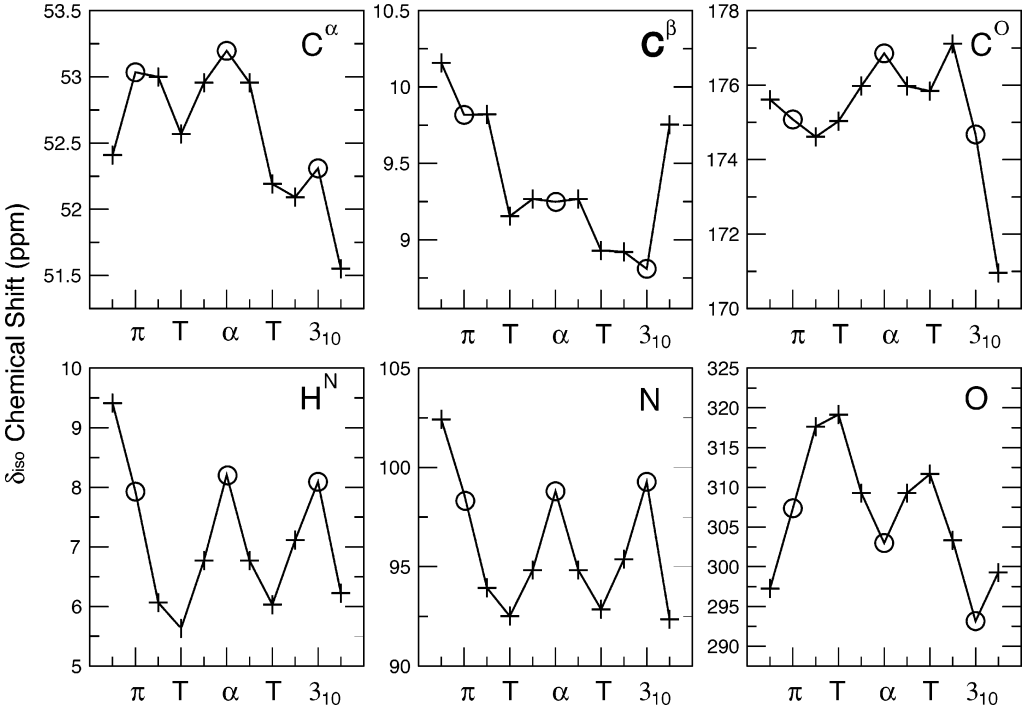

Figure 2. Isotropic chemical shifts δ_{iso} for all atoms in the π, α, 3_{10}, and transitions states "*T*" from one minimum to another along the PES. Refer to Table 4 for numerical values.

TABLE 3: Helical and FES Structure Parameters for the Fully Relaxed Structures along the PES (*T* Refers to a Transition State from Minimum to Minimum), Including Helix Structure Values (*L* and θ , See Figure 1), Torsion Angles (ω, ϕ, ψ), Hydrogen Bonds Values (O−H Distance and Angle COH), the Angle Formed between the $\hat{z}$, Helix Axis and the Bond $\overline{CO}$, and the Hydrogen Bond Energies Published Elsewhere[6]

	L (Å)	θ	ω	ϕ	ψ	O−H (Å)	angle (COH)	angle $\hat{z}$-$\overline{CO}$	E_{hb} (kcal/mol)
π	1.17	80.0	173.0°	−76°	−53°	1.95	153.8°	12.6°	−10.4
$T(\pi-\alpha)$	1.32	83.1	177.3°	−76°	−48°	2.74	146.7°	12.6°	−3.9
α	1.50	98.2	175.2°	−63°	−42°	1.95	148.4°	16.8°	−8.6
$T(\alpha-3_{10})$	1.71	102.9	176.9°	−63°	−36°	2.50	99.11°	12.6°	−3.3
3_{10}	1.95	120.0	179.3°	−60°	−20°	1.92	125.0°	27.1°	−7.7
β	3.57	180.0	177.1°	−60°	164.4°				

TABLE 4: NMR Chemical Shifts in Helical Structures of Relaxed Polyalanine Peptides along the PES Where "*T*" Refers to a Transition State from Minimum To Minimum

model	$\delta^{13}C^{\alpha}$	$\delta^{13}C^{O}$	$\delta^{13}C^{\beta}$	$\delta^{15}N$	$\delta^{1}H^{N}$	$\delta^{17}O$
π	53.04	175.08	9.82	98.66	7.93	307.36
$T(\pi-\alpha)$	52.57	175.03	9.15	92.51	5.63	319.17
α	53.2	176.85	9.25	98.8	8.21	303
$T(\alpha-3_{10})$	52.19	175.84	8.93	92.85	6.03	311.66
3_{10}	52.31	174.68	8.81	99.28	8.09	293.16
FES β	47.32	169.05	12.49	87.62	6.32	286.27
$\lvert\Delta(\alpha-\beta)\rvert$	5.89	7.83	3.25	11.21	1.89	16.49

difference of 1 ppm which, experimentally, may allow discrimination between α and 3_{10} helix, but this difference is within experimental and theoretical uncertainty. Because of its spectral range, the most significant difference in chemical shifts among the minima helical structures are those for δ ^{17}O (Table 4). Nevertheless, in a real scenario, one would expect a combination of three different structures and a range of distorted helical conformations around these minima. Therefore, because of the plots in Figure 2, these differences would not allow us to distinguish between minima and conformations in a transition state from a minimum to the other.

From the theoretical values, one could note certain structural features. For example, the differences $\Delta(\alpha - \text{FES})$ for H, N, and O are 1.89, 11.21, and 16.49 ppm, respectively, denoting the formation of hydrogen bonds as the FES structures represent simply an isolated β strand with no hydrogen bonds in between. In general, one might expect the ^{1}H chemical shift to be the most direct observable for identifying hydrogen bonding. This is because of hydrogen's high gyromagnetic constant and its abundance in nature. However, in the case of discriminating between helical structures, the results in Figure 2 suggest that oxygen provides the biggest differences in chemical shift between helical structures. This is not just because of the large range of chemical shift (−50−900 ppm) but also because δ ^{17}O is involved in the hydrogen bonding in the helical structures. Benefits of ^{17}O parameters derived from solid-state NMR for describing hydrogen bonds have already been described.[33−35] Therein, it has been suggested that changes in chemical shift can potentially be used to monitor changes in hydrogen bonding and the protonation state of a molecule. Comparison with similar chemical shift ranges of organic molecules measured in solution shows significant differences up to 100 ppm. This is mainly due to changes in the hydrogen-bond network.

Experimentally, nuclei with spin-1/2 have been preferred for NMR spectroscopy because good resolution can be obtained in complex protein systems, and a large range of experiments can be used to obtain information about distances and bonding between neighboring atoms. In terms of an appropriate experimental procedure to use ^{17}O for determining helical structures, as ^{17}O is a rare nuclei with a natural abundance of 0.037%, it is believed that the only way to achieve site selectivity would be by isotopic labeling, primarily because of sensitivity or more

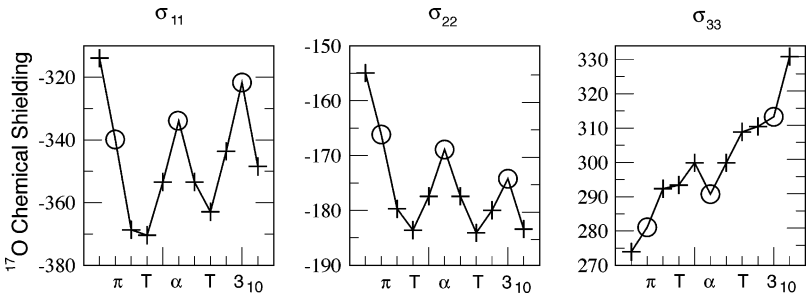

Figure 3. Anisotropic chemical shielding for ^{17}O in the π, α, 3_{10}, and transitions states "*T*" from one minimum to another along the PES.

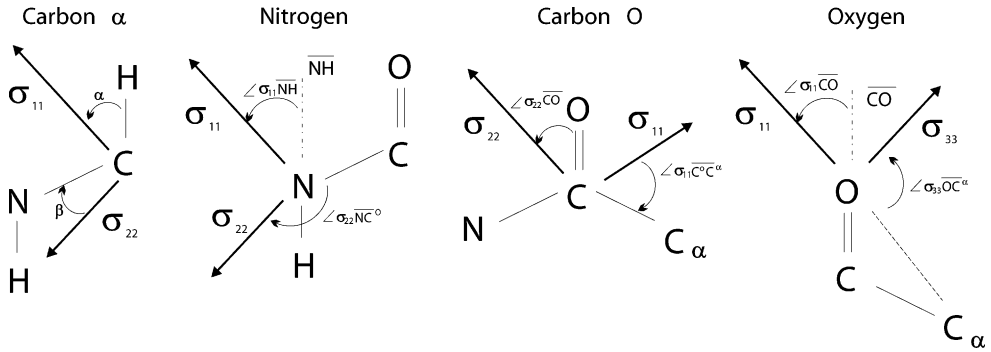

Figure 4. Schematic representations of the angles between the orientation of main components of the CSA tensor and molecular bonds, reference to Table 5.

TABLE 5: Angles between the Orientation of Main Components of the Chemical Shift Tensor and Molecular Bonds for π, α, and 3_{10} Helix Structures as Described in Figure 4

	angle	π	α	3_{10}
C^{α}	α	63.13°	64.77°	51.39°
	β	42.13°	43.21°	46.61°
N	$\angle\sigma_{11}\overline{NH}$	18.6°	17.3°	18.8°
	$\angle\sigma_{22}\overline{NC^{O}}$	64.96°	64.06°	57.79°
C^{O}	$\angle\sigma_{22}\overline{CO}$	2.8°	3.15°	2.8°
	$\angle\sigma_{11}\overline{C^{O}C^{\alpha}}$	29.0°	31.72°	28.3°
O	$\angle\sigma_{11}\overline{CO}$	8.26°	8.3°	5.87°
	$\angle\sigma_{33}\overline{OC^{\alpha}}$	88.89°	88.8°	87.8°

specifically the signal-to-noise ratio (*S*/*N*) as well as the gyromagnetic ratio, which determines the Larmor frequency of the nucleus at a particular magnetic field. However, it has been demonstrated by Wong et al.[36] that one does not need selective labeling as all ^{17}O sites in monosodium glutamate are resolved by MAS double-rotation (DOR) experiments, and the static line width is determined by the EFG and CSA. Besides, direct ^{17}O dipolar coupling is very small in solid-state NMR, and contrary to the liquid state, low abundance is an advantage since it reduces dipolar coupling effects where high natural abundance would lead to static line broadenings in the order of 50 kHz. ^{17}O is favorable for studies by solid-sate NMR experiments because it is a quadrupolar nucleus with a half-integer spin $I = 5/2$.[33] From these experimental and theoretical advantages, ^{17}O appears to be the best nucleus to use in NMR experiments for discriminating between different helix structures. Nevertheless, information is required for the specific task of discriminating between very small structural differences in helical structure. This essential information will be investigated below through the anisotropy of chemical shifts.

Anisotropy of the Chemical Shielding. Prior to discussing the anisotropic chemical shielding tensors of our systems, one should note that each hydrogen bond in a helical structure has a highly oriented dipole moment. In finite models without periodic conditions, the oriented dipoles sum up to generate a "macrodipole''. This macrodipole may cause spurious but strong anisotropies. In a real protein environment, such a macrodipole is compensated by the presence of charged amino acids or by the solvent. In our calculations, this artificial effect, which can arise in finite models, is avoided by the use of periodic boundary conditions. Although we are not artificially enhancing the anisotropies, they do introduce important differences between the three helical environments demonstrated by Figure 3.

TABLE 6: Theoretical and Experimental EFG Parameters: the Quadrupolar Coupling Constant C_Q and the Asymmetry Parameter η_Q for the Three Helix Minima Structures of Polyalanine Peptide

model	C_Q^{The} (MHz)	η_Q^{The}	C_Q^{Exptl} (MHz)	η_Q^{Exptl}
π	9.378	0.243		
α	9.200	0.260	8.59[42]	0.28[42]
3_{10}	8.935	0.291		

Experimentally, structural differences between α helix and β strand have been studied by means of δ_{22} $^{13}C^{O}$ and ^{15}N CSA tensors[17,37−39] and has proven to offer the relevant information. In this work, we restrict ourselves to the study of the ^{17}O CSA since it was found to be the only nucleus which shows major differences between helices. Figure 3 represents anisotropic chemical shielding for ^{17}O in different conformations. In this plot, σ_{33} ^{17}O is the component of the CSA tensor which shows the biggest differences between the helices. This component is perpendicular to the CO bond, points toward the center of the helix, and shows a difference of 20 ppm between the α and the 3_{10} helix. Because of the well-defined pattern of ^{17}O σ_{33}, one could differentiate between very small changes in the helical conformation. Around the α region, however, it would be impossible to discern any minor distortions. For the rest of the points along this plot, this observable shows very well-defined differences and offers information about tiny changes in the structure.

The orientation of the principal components of the shielding tensor for some atoms of the peptidic unit in the helical models are given in Table 5. The accuracy of the ab initio calculation

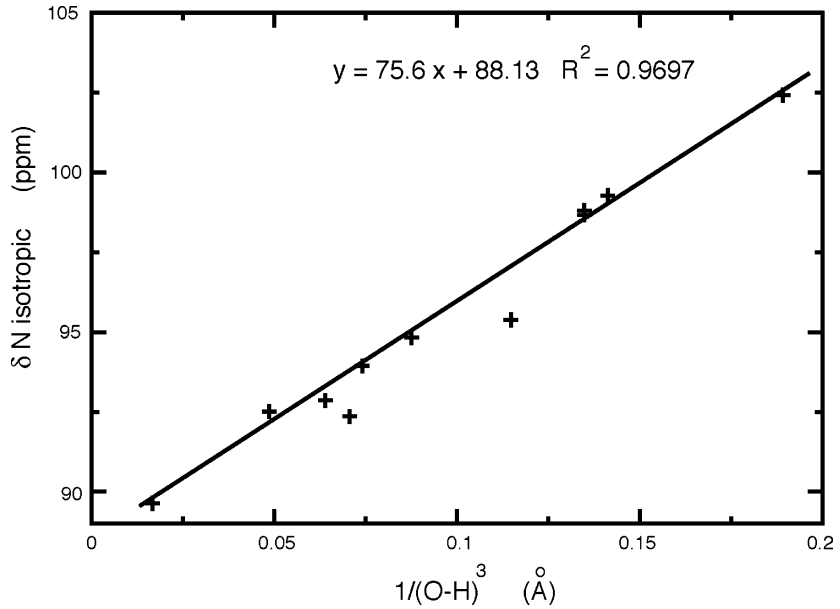

Figure 5. Correlation between the inverse of the cubic hydrogen bond distance (O−H) and the isotropic ^{15}N chemical shift.

of these observables is very high according to previous work,[40] and relevant information can be extracted. The C^{α} orientation is presented using the convention of ref 41 which is schematically depicted in Figure 4: for N and C^{O}, the vectors $\overrightarrow{NH}$ and $\overrightarrow{CO}$ are almost parallel to the helical axis. In these cases, the third principal component of the shielding tensor can be obtained by the orthogonality condition. For C^{α}, one can see from Figure 4 that the orientation of σ_{11} relative to the C−H bond changes only slightly between the α and the π structures but that there is a substantial reorientation of around 7° for the 3_{10} structure. This reorientation could be useful for distinguishing 3_{10} from the other two structures. In contrast, the angle β only shows a small difference between the three helical structures but a clear similarity between π and α. For nitrogen, the orientation of σ_{33} with respect to $\overrightarrow{NH}$ changes 1° at most among the different structures, whereas the orientation of σ_{22} with respect to the $\overrightarrow{NC}$ direction changes appreciably only between the 3_{10} and the other two structures. For the oxygen atom, the angle between the σ_{33} component and the helical axis increases in the order $\pi < \alpha < 3_{10}$ which is opposite to that of the σ_{22} and $\overrightarrow{OC}$ direction (Table 5).

By performing experimental analysis of the solid-state ^{17}O NMR spectrum, one can obtain the relative orientation between the EFG and the chemical shielding tensor. Technically, this is difficult because it requires the absolute tensor orientation to be obtained relative to the experimental framework. The EFG's directions are not reported because it is beyond the main focus of this study, but these can be obtained upon request from the authors. The calculated and theoretical values of quadrupolar coupling C_Q and the asymmetry parameter η_Q are presented in Table 6. Despite the poor fit to the experimental data, one could try to find some trends between different structures, but the three helical structures have very similar asymmetry parameters η_Q which would suggest that measurement of this quantity would not be very useful for differentiating among helical structures. However, there are greater variations in C_Q, which show the same trends as the δ^{17}O, decreasing from π to 3_{10}. This agrees with previous findings that C_Q decreases with increasing hydrogen bond strength.[30]

Effect of the Hydrogen Bond Distance. In helical conformations, hydrogen bonds are highly present and are the main stabilizing forces. Additionally, different conformations of these bonds yield different values of chemical shift. It is therefore tempting to look for a correlation between hydrogen bonding and chemical shifts. Quantifying the strength of the hydrogen bond is however a very difficult task. For helix structures along the minimum energy pathway, the hydrogen bond varies in distance and angles as shown in Table 3 (see also Figure 4 in ref 6). The only parameter that was found with reasonable correlation was the inverse of the cubic of the distance H−O between the hydrogen and the oxygen forming the hydrogen bond. Figure 5 shows a plot of calculated δ N chemical shifts against $1/(H - O)^3$. This shows a general trend whereby increased hydrogen bond strength results in a decreased shielding of the nitrogen. The value of the linear regression coefficient is $R^2 = 0.9697$. Although this is a very good fit, it would be interesting to see if the differences are large enough to allow measurements to distinguish the different helical structures in real experimental situations.

A similar trend was found for δ H chemical shifts following the inverse of the cubic of the hydrogen−oxygen distance (O−H). The linear expression is $\delta_H = 2.823/(O-H)^3 + 75.89$ with a regression coefficient of $R^2 = 0.9757$. Interestingly, none of the oxygen isotropic or anisotropic chemical shift tensors show a linear regression with a specific structural parameter.

It has been shown that the hydrogen bond is a good reaction coordinate for describing the structural transitions between helical conformations.[6] Thus, the correlation between isotropic δ_N and δ_H may be helpful in identifying the helical conformation present in a protein sample.

5. Conclusion

It has been shown that theoretical calculations of ^{17}O, ^{15}N, and ^{13}C chemical shieldings in molecules with periodic boundary conditions are very sensitive to the local intermolecular hydrogen-bonding interactions. In particular, this sensitivity has been exploited to show that experimental measurements can discriminate between helix structures in mono-polypetides of alanine. The σ_{33}^{O} chemical shift anisotropy of these structures varies by as much as 10 ppm between π and α and 20 ppm between α and 3_{10}. For NMR data, σ_{33}^{O} was found to be the most important parameter for discriminating among helical

structures. A review and discussion of other experimental observables was also presented in order to elucidate their behavior and to identify their utility in distinguishing helical structures. It was shown that the direction of the principal axis is extremely sensitive to minor changes in structure and that this can be used to distinguish among helical conformations and orientation of transmembrane helical peptide.

Acknowledgment. Computational resources were provided by the Cambridge-Cranfield High Performance Computing Facilities. We would like to thank Professor Ray Dupree for very helpful comments and discussion on this article. M.G. acknowledges CONACYT for financial support through Project No. 49057.

References and Notes

(1) Barlow, D. J.; Thornton, J. M. *J. Mol. Biol.* **1988**, *201*, 601−619.
(2) Weaver, T. M. *Protein Sci.* **2000**, *9*, 201−206.
(3) Freedberg, D. I.; Venable, R. M.; Rossi, A.; Bull, T. E.; Pastor, R. W. *J. Am. Chem. Soc.* **2004**, *16*, 10478−10484.
(4) Wuthrich, K. *NMR Proteins and Nucleic Acids;* John Wiley and Sons: New York, 1986.
(5) Jaravine, V. A.; Alexandrescu, A. T.; Grzesiek, S. *Protein Sci.* **2001**, *10* (5), 943−950.
(6) Ireta, J.; Neugebauer, J.; Scheffler, M.; Rojo, A.; Galvan, M. *J. Am. Chem. Soc.* **2005**, *127* (49), 17241−17244.
(7) Pickard, C. J.; Mauri, F. *Phys. Rev. B* **2001**, *6324*, 245101−13.
(8) Dedios, A. C.; Pearson, J. G.; Oldfield, E. *Science* **1993**, *260*, 1491−1496.
(9) Heitmann, B.; Job, G. E.; Kennedy, R. J.; Walker, S. M.; Kemp, D. S. *J. Am. Chem. Soc.* **2005**, *127*, 1690−1704.
(10) Ireta, J.; Neugebauer, J.; Scheffler, M.; Rojo, A.; Galvan, M. *J. Phys. Chem. B* **2003**, *107*, 9616−9616.
(11) Wieczorek, R.; Dannenberg, J. J. *J. Am. Chem. Soc.* **2003**, *125* (27), 8124−8129.
(12) Wu, Y. D.; Zhao, Y. L. *J. Am. Chem. Soc.* **2001**, *123* (22), 5313−5319.
(13) Improta, R.; Barone, V.; Kudin, K. N.; Scuseria, G. E. *J. Am. Chem. Soc.* **2001**, *123* (14), 3311−3322.
(14) Bogar, F.; Szekeres, Z.; Bartha, F.; Penke, B.; Ladik, J. *Phys. Chem. Chem. Phys.* **2005**, *7* (15), 2965−2969.
(15) Long, H. W.; Tycko, R. *J. Am. Chem. Soc.* **1998**, *120*, 7039−7048.
(16) Lee, D. K.; Ramamoorthy, A. *J. Phys. Chem. B* **1999**, *103*, 271−275.
(17) Shoji, A.; Ozaki, T.; Fujito, T.; Deguchi, K.; Ando, S.; Ando, I. *J. Am. Chem. Soc.* **1990**, *112*, 4693−4697.
(18) Havlin, R. H.; Laws, D. D.; Bitter, H. M. L.; Sanders, L. K.; Sun, H. H.; Grimley, J. S.; Wemmer, D. E.; Pines, A.; Oldfield, E. *J. Am. Chem. Soc.* **2001**, *123*, 10362−10369.
(19) Kohn, W.; Sham, L. *Phys. Rev.* **1965**, *140* (4A), 1133−1138.
(20) Perdew, J. P.; Burke, K.; Ernzerhof, M. *Phys. Rev. Lett.* **1996**, *77* (18), 3865−3868.
(21) Troullier, N.; Martins, J. *Phys Rev B* **1991**, *43* (3), 1993−2006.
(22) Bockstedte, M.; Kley, A.; Neugebauer, J.; Scheffler, M. *Comput. Phys. Commun.* **1997**, *107*, 187−222.
(23) Calculations were performed with PARATEC (PARAllel Total Energy Code) by Pfrommer, B.; Raczkowski, D.; Canning, A.; Louie, S. G. Lawrence Berkeley National Laboratory (with contributions from Mauri, F.; Cote, M.; Yoon, Y.; Pickard, C.; and Haynes, P.); for more information, see www.nersc.gov/projects/paratec.
(24) Monkhorst, H. J.; Pack, J. D. *Phys. Rev. B* **1976**, *13*, 5188−5192.
(25) Haeberlen, U. *High Resolution NMR in Solids: Selective Averaging;* Academic Press: New York, 1976.
(26) Asakawa, N.; Kurosu, H.; Ando, I. *J. Mol. Struct.* **1994**, *323*, 279−285.
(27) Profeta, M.; Mauri, F.; Pickard, C. *J. Am. Chem. Soc.* **2003**, *125*, 541−548.
(28) Pyykko, P. *Mol. Phys.* **2001**, *99* (19), 1617−1629.
(29) Yates, J. R.; Dobbins, S. E.; Pickard, C. J.; Mauri, F.; Ghi, P. Y.; Harris, R. K. *Phys. Chem. Chem. Phys.* **2005**, *7*, 1402−1407.
(30) Yates, J. R.; Pickard, C. J.; Payne, M. C.; Dupree, R.; Profeta, M.; Mauri, F. *J. Phys. Chem. A* **2004**, *108*, 6032−6037.
(31) Fletterick, W.; Tsai, C. C.; Hughes, R. E. *J. Phys. Chem.* **1971**, *75*, 918−922.
(32) Trevino, S. F.; Prince, E.; Hubbard, C. R. *J. Chem. Phys.* **1980**, *73* (6), 2996−3000.
(33) Lemaitre, V.; de Planque, M. R. R.; Howes, A. P.; Smith, M. E.; Dupree, R.; Watts, A. *J. Am. Chem. Soc.* **2004**, *126*, 15320−15321.
(34) Lemaitre, V.; Smith, M. E.; Watts, A. *Solid State Nucl. Magn. Reson.* **2004**, *26*, 215−235.
(35) Pike, K. J.; Lemaitre, V.; Kukol, A.; Anupold, T.; Samoson, A.; Howes, A. P.; Watts, A.; Smith, M. E.; Dupree, R. *J. Phys. Chem. B* **2004**, *108*, 9256−9263.
(36) Wong, A.; Howes, A. P.; Pike, K. J.; Lemaitre, V.; Watts, A.; Anupold, T.; Past, J.; Samoson, A.; Dupree, R.; Smith, M. E. *J. Am. Chem. Soc.* **2006**, *128* (24), 7744−7745.
(37) Wei, Y. F.; Lee, D. K.; Ramamoorthy, A. *J. Am. Chem. Soc.* **2001**, *123*, 6118−6126.
(38) Asakawa, N.; Kuroki, S.; Kurosu, H.; Ando, I.; Shoji, A.; Ozaki, T. *J. Am. Chem. Soc.* **1992**, *114*, 3261−3265.
(39) Kameda, T.; Takeda, N.; Kuroki, S.; Kurosu, H.; Ando, S.; Ando, I.; Shoji, A.; Ozaki, T. *J. Mol. Struct.* **1996**, *384*, 17−23.
(40) Sefzik, T. H.; Turco, D.; Luliucci, R. J.; Facelli, J. C. *J. Phys. Chem.* **2005**, *109*, 1180−1187.
(41) Jameson, C. J. *Solid State Nucl. Magn. Reson.* **1998**, *11*, 265−268.
(42) Yamauchi, K.; Kuroki, S.; Ando, I.; Ozaki, T.; Shoji, A. *Chem. Phys. Lett.* **1999**, *302* (3−4), 331−336.
(43) Hartzell, C. J.; Whitfield, M.; Oas, T. G.; Drobny, G. *J. Am. Chem. Soc.* **1987**, *109*, 5966−5969.